Revue des Composites et des Matériaux Avancés-Journal of Composite and Advanced Materials
Vol. 36, No. 5, October, 2026, pp. 1145-1158
Journal homepage: http://iieta.org/journals/rcma

High Temperature Aging-Induced Degradation of Super 304H Stainless Steel Welds: A Microstructural and Mechanical Comparison Between TIG and SMAW

Thanaa Abdel Salam Tawfiq[1], Mohammed Sabeeh Mohammed[2*], Mousa Alaa Hussein[3], Noor Jalil Nader Nasser[4], Samir Ali Amin[5], Laith Jaafer Habeeb[2]

[1] Polytechnic College for Engineering, Middle Technical University, Baghdad 10074, Iraq
[2] Training and Workshop Center, University of Technology-Iraq, Baghdad 10066, Iraq
[3] College of Civil Engineering, University of Technology-Iraq, Baghdad 10066, Iraq
[4] Department of Aeronautical Technical Engineering, College of Technical Engineering, Al-Farahidi University, Baghdad 10001, Iraq
[5] Department of Mechanical Power Techniques Engineering, Refrigeration and Air-conditioning, College of Technical Engineering, Al-Farahidi University, Baghdad 10001, Iraq

Corresponding Author Email: Mohammed.s.mohammed@uotechnology.edu.iq

Copyright: ©2026 The authors. This article is published by IIETA and is licensed under the CC BY 4.0 license (http://creativecommons.org/licenses/by/4.0/).

https://doi.org/10.18280/rcma.360520

Received: 27 May 2026
Revised: 31 July 2026
Accepted: 12 August 2026
Available online: 31 October 2026

Keywords:
carbide precipitation, Charpy impact testing, high-temperature aging, microstructural evolution, Super 304H stainless steel

ABSTRACT

This study compares the microstructural changes and mechanical degradation in Super 304H austenitic stainless steel butt welds subjected to long-duration high-temperature thermal aging. The 5 mm-thick plates were welded to form joints by Tungsten Inert Gas (TIG) welding with 1.6 mm-diameter Super 304H filler wire in 99.9% argon shielding, and by Shielded Metal Arc Welding (SMAW) using a 3.2 mm-diameter E308-16 flux-coated electrode. Triplicate specimens (three for each condition) were isothermally aged at 650 ℃ for 500 hours and then air-cooled. Mechanical behavior was directly affected by secondary-phase precipitation, as evidenced by scanning electron microscopy (SEM), transmission electron microscopy (TEM), energy-dispersive X-ray spectroscopy (EDS), and selected-area electron diffraction (SAED). The fine-grained austenitic matrix obtained by TIG welding, combined with low heat input and high cooling rates, led to controlled, dispersed precipitation of M23C6 carbide along grain boundaries. Conversely, SMAW had a higher heat input and a slower cooling rate, resulting in coarser grain sizes and wider intergranular carbide networks, especially in localized ferritic areas. Moderate reductions in toughness (14.1%) were observed in the TIG-welded joints (a reduction in the sub-size Charpy V-notch tests from 213 J/cm² as-welded to 183 J/cm² welded). On the other hand, the SMAW weld exhibited more severe embrittlement; toughness dropped by 20.2% from the SMAW base metal (BM) (198 J/cm²) to 158 J/cm². Microhardness measurements along the BM, the heat-affected zone (HAZ), and the fusion zone (FZ) showed that SMAW joints had peaks at higher values that were attributed to coarse carbide agglomeration. In contrast, TIG welds had a uniform profile with a peak value of 205 HV. Based on the observed carbide morphology, it was suggested that TIG welds have a lower intergranular sensitization potential than SMAW welds. However, no direct corrosion testing was conducted.

1. INTRODUCTION

The impact toughness of austenitic stainless steel weld metal is strongly affected by the kinetics of intergranular precipitation in high-temperature use. Since this material is widely used in critical applications such as heat exchangers and pressure vessels in ultra-supercritical boiler systems, it is important to study the effects of these precipitates on its mechanical properties. Intergranular precipitation of carbides and other secondary phases at grain boundaries can significantly degrade steel toughness by facilitating localized brittle fracture. The precipitation processes, including the growth and distribution of particle-like M23C6 carbides, are central to altering the microstructure and, consequently, the resistance to impact loading. Purzyńska et al. [1] analyzed the long-term behavior of austenitic Super 304H steel after 31000 hours of operation at 570 ℃. Their microstructural examination shows severe precipitation of M23C6 carbides and sigma-phase particles at grain boundaries, along with dispersed ε-Cu and MX particles in grains. Wu et al. [2] explored strengthening and embrittling mechanisms of Super 304H steel under extended aging at 650 ℃ by considering the precipitates in the material microstructure. Their results show that the increase in hardness attributed to the M23C6 carbides at grain boundaries and intragranular nano-Cu-rich particles is critical to the increases in hardness of about 10 HV and 30 HV,

respectively, after 5000 hours. Zieliński et al. [3] examined the long-term aging degradation of Super 304H steel exposed to aging for up to 50,000 hours at 650 ℃ and 750 ℃, and study the microstructure. The precipitation of various phases, such as M23C6, MX carbides, σ phase, Z phase, and ε-Cu phase, which significantly influence the creep strength of the materials, is reported in their findings. The study shows that elevated temperature is a critical factor in altering the steel's microstructure and, therefore, its mechanical behavior. Xiao et al. [4] investigated the influence of Nb addition on microstructural changes and microhardness in Super 304H austenitic stainless steel weld metals during long-term aging at 650 ℃. Their work indicates that, while Nb-free weld metal displays nanoscale M23C6 particles in the interdendritic regions, Nb-bearing weld metal has coarsened M23C6 particles at the phase interfaces between the primary Nb(C, N). Both weld metals are known to exhibit coarsening of Cu-rich particles with time. Li and Wang [5] examined the influence of second-phase precipitation on the mechanical properties of 22Cr25Ni3W3CuCoNbN steel, a new heat-resistant steel for superheaters in A-USC boilers. Their analysis reveals that exposure to aging at 700 ℃ for up to 1000 hours results in significant precipitation of the M23C6 carbides, initially preferentially at grain boundaries, thereby decreasing impact toughness. Zhao et al. [6] studied the long-term performance of Super 304H and HR3C steels after 40,000 hours of service at 630 ℃ and 3 MPa with respect to their oxidation behavior. The study shows the development of duplex oxides on the exposed steel surface, while surface deformation in Super 304H increases its corrosion resistance. M23C6 carbides, NbCrN, and ε-Cu precipitates are found at the grain boundaries and inside the grains for Super 304H, and Cr aggregation with nanoscale NbCrN particles in the grains is found for HR3C. Tikhonova et al. [7] examined the effect of increasing age up to 3000 h at 923 K on the structure, additional phases, strength, and intergranular detrimental corrosion of the Super 304H austenitic stainless steel. Their work shows that after 100 hours of aging, M23C6 carbides form at grain boundaries, and these boundaries broaden over time, increasing the likelihood that the material will become brittle and susceptible to intergranular corrosion. Xiao et al. [8] studied the effect of intergranular precipitation behavior on stress relaxation cracking susceptibility of Super 304H austenitic stainless steel weld metal during long-term aging. Their study shows that M23C6 carbides selectively precipitate at 45° misorientation grain boundaries, where they exhibit lower nucleation energy and higher strain concentration, making them prone to stress-relaxation cracking. Jin et al. [9] studied microstructural transformation and its role in the development of mechanical characteristics during aging of Super 304H steel at 650 ℃. The precipitation of Cu-rich, MX, M23C6, and σ particles is identified, with nano Cu-rich and MX particles distributed in the matrix and micron-sized M23C6 and σ particles formed at grain boundaries. The results show that with aging, tensile strength and hardness increase, whereas impact energy decreases, especially at two stages. Dash et al. [10] investigated the microstructural evolution and mechanical properties of Super 304H Cu-grade austenitic stainless steel (SS Super 304HCu) during long-term thermal exposure. Their work detected grain-boundary primary Nb(C, N) and M23C6 precipitates, secondary Nb(C, N) carbides, and Cu-rich phases that remained uniform over 10,000 hours of aging at 630 ℃. The results show that the creep rate increases significantly at higher temperatures, but as the Cu-rich phase precipitates, creep resistance also improves. Pulford et al. [11] examined elevated-temperature (650 ℃ and 700 ℃) uniaxial creep rupture specimens of the Super 304H austenitic stainless steel (Super 304H) and the microstructural evolution in the specimens. Their phase analysis focused on the precipitation of other second-phase products and a distinctly increased number of nanoscale Nb-rich and Cu-rich particles in the 700 ℃ specimens. Most importantly, the researchers demonstrated a direct spatial relationship between the formation of the brittle sigma phase and the formation of creep cavities. Kumar et al. [12] studied the impact of modified post-weld heat treatment (PWHT) processes on the mechanical properties and microstructure of dissimilar welded joints of T91 and Super 304H. Using Tungsten Inert Gas (TIG) welding, they performed two variants of PWHT processes: post-weld normalizing and tempering (PWNT) and post-weld direct tempering (PWDT). Results reveal enhanced microstructural uniformity and reduced Cr carbides in PWNT, whereas smaller carbides and sensitization occur on the Super 304H side in PWDT.

Hwang et al. [13] investigated the tensile and fatigue properties of Super 304H welding joints at high temperatures (500–700 ℃), a temperature range important for heat exchangers in thermal power plants. The research indicates that the tensile strength of welding joints equals that of the base metal (BM) at all tested temperatures. Still, substantial shrinkage in deformation is observed due to non-uniform deformation. The high-temperature aging behavior of Super 304H austenitic steel, with particular focus on the coarsening and hardening of copper-rich precipitates at aging temperatures between 650 and 750 ℃, was investigated by Ou et al. [14]. They focused on the microstructures and revealed that these particles remain coherent and maintain a cubic-to-cubic crystallographic relationship with the matrix at longer exposure times. Still, their growth rate is primarily controlled by the diffusion volume of copper atoms. Jiang and Zhu [15] examined the strengthening mechanism of precipitates in S30432 heat-resistant steel under short-term aging at 923K, specifically in Cu-rich particles. Their work identifies Cu-rich particles as the major contributors to steel yield strength, accounting for at least 60% of the strengthening effect, ahead of Nb(C, N) and M23C6 particles. Although the degradation of the microstructures of copper-alloyed and niobium-alloyed Super 304H base materials after long periods of service (above 10,000 hours) has been well documented in the literature, there is a critical lack of understanding of the intermediate aging behavior of Super 304H weldments. The microstructural evolution of weld metal is fundamentally different from that of its BM due to the unique dendritic solidification pattern, elemental segregation, and welding thermal effects during the welding cycle. In addition, no studies have specifically identified these degradation pathways and separated the effects that the arc welding methodology has on them. The different levels of heat input and weld cooling rates associated with TIG and Shielded Metal Arc Welding (SMAW) processes result in different initial grain sizes and phase distributions, for example, localized retention of delta-ferrite. Hence, the objective of this work is to directly compare the microstructural and mechanical degradation of Super 304H stainless steel joints welded by TIG and SMAW with Super 304H and E308-16 consumables, respectively. This study subjects these joints to a controlled 500-hour thermal treatment at 650 ℃, thereby revealing the effects of the specific thermal cycles of each welding process on the

precipitation of intergranular M23C6 carbide, and on the control of that carbide and its relation to the subsequent drop in impact toughness and local hardenability. In industrial applications, it is important to note that the welding methodology and the choice of filler material are closely interlinked. Accordingly, each of the welding configurations (TIG with the Super 304H filler, SMAW with the E308-16 filler) is treated as a separate 'Welding System,' and the synergistic effects of the thermal cycle and chemistry are assessed for long-term aging resistance.

2. EXPERIMENTAL PROCEDURE

2.1 Welding joint samples preparation

304 stainless steel plates 5 mm thick were used as the BM for butt welding joints. Three samples were welded using two arc-welding techniques: SMAW and TIG.

A 650 ℃-solution heat treatment for 500 hours was then performed, followed by air cooling. SMAW used a 3.2-mm-diameter E308-16 electrode manufactured by ESAB. The TIG filler rod used with TIG was Super 304H, manufactured by ESAB, with a diameter of 1.6 mm. The chemical compositions of the BM and filler wire are shown in Table 1. Super 304H filler has been selected instead of the BM; manganese and nickel contents have been increased, and approximately 1 wt.% Molybdenum has been chosen [16]. A multi-pass gas tungsten arc welding process was used to prepare the weld metal under investigation. The groove form is a V-shaped groove with a 1.6 mm gap and a 1 mm root face. The butting groove was processed to 30–35°, as shown in Figure 1. The investigated welding parameters are shown in Tables 2 and 3.

Table 1. Base metal (BM), Shielded Metal Arc Welding (SMAW), and Tungsten Inert Gas (TIG) filler wire chemical compositions (wt.%)

Element	Base Metal (BM)	Super 304H Filler	E308-16
C	0.062	0.14	0.06
Cr	18.06	17.7	19.6
Si	0.45	0.21	0.58
Mo	0.18	0.95	-----
Ni	8.67	17.11	10.2
Mn	0.83	3.21	1.6
N	0.128	0.31	----
Nb	0.32	0.73	----
Cu	2.76	3.05	----
S	0.005	0.004	≤0.03
P	0.018	0.006	≤0.03

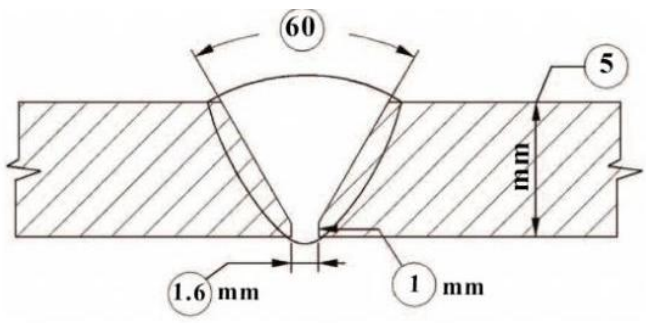


Figure 1. Welding joint design dimensions

Table 2. Tungsten Inert Gas (TIG) welding parameters and conditions

Parameter	Specification
Filler Type	Super 304H
Welding Current	100 A
Arc Voltage	12 V
Shielding Gas	Argon (99.9% pure)
Filler Wire Diameter	1.6 mm
Travel Speed	200 mm/min
Torch Angle	20° from vertical
Flow rate	15 L/min

Table 3. Shielded Metal Arc Welding (SMAW) welding parameters and conditions

Parameter	Specification
Electrode Type	E308-16
Current	90–130 A (for 5 mm thickness)
Voltage	25 V
Arc Length	Maintain arc length between 3 and 5 mm for optimal stability
Shielding Gas	No external gas is required because SMAW uses flux-coated electrodes
Travel Speed	20 cm/min (depending on weld bead size and joint fit-up)
Electrode Diameter	3.2 mm

2.2 Aging samples test

Welded specimens from TIG and SMAW welders were prepared for the aging test by taking 55 mm-long samples from the joint, with the seam placed at the center of each sample. After that, the samples were aged for 500 hours at 650 ℃. To analyze the microstructural evolution and sensitization susceptibility of the weldments, the weld joints of the samples were observed using optical microscopy and scanning electron microscopy (SEM).

2.3 Microstructure test characterization

Welded metal cross-sections were utilized to obtain samples for microstructural examination. The samples underwent grinding, polishing, and rust removal before microscopic analysis using OMM-9XB-PC metallurgical microscopes and a Zeiss EVO MA10 with an EDAX energy-dispersive X-ray spectroscopy (EDS) spectrometer and SEM. Figure 2 presents the microstructural characterization of the sample location around the weld seam center (dashed rectangular box). EDS was employed to analyze the chemical composition at several sites to identify precipitate types. Further phase, precipitate, and characterization investigations were conducted using an HT7700 transmission electron microscopy (TEM). While it is inferred from the visual morphology and the detail of the subsequent etching during the optical and electron microscopy that the thresholds of 1204 ℃ for the SMAW heat-affected zone (HAZ) gave rise to localized formation of the delta-ferrite phase and 1205 ℃ for the TIG fusion zone (FZ) to the formation of possibly trace amounts of martensite, quantitative phase measurements (e.g., X-ray Diffraction or Electron Backscatter Diffraction) and Ferrite Number (FN) measurements were not performed within the scope of this work. The specific structure changes of these macroscopic phases, therefore, are to be interpreted as microstructural inferences. These are based on the well-known metallurgical

principles of austenitic stainless steels and on the character of the thermal cycles obtained with the different welding processes (as predicted by compositional equivalents, according to the Schaeffler diagrams and WRC-1992).

2.4 V-notch impact test

A V-notch was machined directly into the center of the FZ, parallel to the longitudinal centerline of the weld seam (Figure 2). The samples obtained (10 mm × 7.5 mm × 55 mm) were subjected to a Charpy V-notch impact test under ambient conditions. All three test specimens (n = 3) were investigated for each aging condition to minimize experimental error and ensure repeatability. The obtained data are presented as the mean value ± standard deviation. The microstructure of the bread surfaces was examined using SEM, which provides insight into the fracture mechanisms.

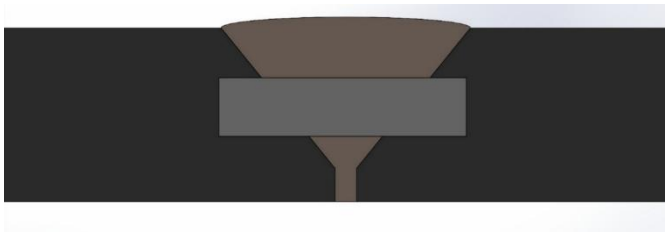


Figure 2. Impact sample and microstructural characterization sample location

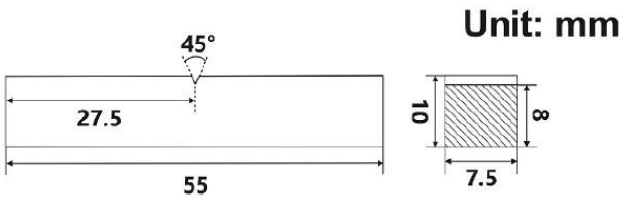


Figure 3. Impact sample dimensions

Measured impact energy (E) in Joules was divided by the net area of a fracture below the notch ligament (A = 0.6 cm^2), and impact toughness was reported in units of (J/cm^2) to enable consistent comparison of results between different joint configurations. Testing was conducted in accordance with American Society for Testing and Materials (ASTM) E23 [16] for sub-size specimens, as shown in Figure 3.

2.5 Vickers microhardness

To conduct a microhardness survey across the HAZ and welding zone for each welded sample, a Vickers microhardness tester was used. The load from the machine was 100 gf, with a 500 µm interval between each mark. The welding joint and HAZ metallographic specimens were placed in a flat position. Measurements were performed in accordance with ASTM E384 [17]. The hardness test procedure included the hardness traverse line at mid-thickness of the section, traversing the unaffected BM, HAZ, and the FZ, a total of 30 indents.

2.6 Transmission electron microscopy, selected area electron diffraction, and energy-dispersive X-ray spectroscopy analysis

The precipitates and phases were also analyzed and identified using the JEM-2010 TEM. All reproductions of extraction TEM samples were prepared by spraying a fine carbon feather on the sample surface, followed by etching the sample in aqua regia to dislodge the matrix. TEM thin foils were manufactured through a twin-jet electropolishing process at 30 V in 10% $HClO_4$ and 90% CH_3COOH electrolyte at 30 °C. Using selected area electron diffraction (SAED) Analysis, the authors examined the various levels occurring during the welding process, how these levels changed over time, the interaction between intergranular precipitates and the matrix, and their impact on the welding process.

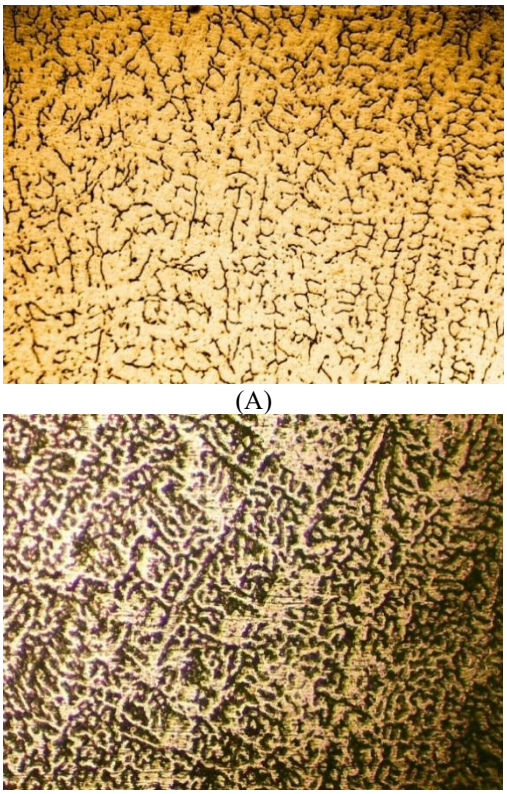
3. RESULTS AND DISCUSSIONS

3.1 Welding zone microstructure analyses

TIG welding and SMAW are welding processes that involve high heat, allowing materials to be melted together. All operational parameters, i.e., heat input, cooling rate, and shielding mode, directly influence the microstructure and mechanical behavior of the weld zone. A comprehensive understanding of these variations is necessary to optimize processes. When each technique is applied to Super 304H stainless steel, Figures 4(A) and (B) show the resulting weld zones. The welding parameters, shown in Tables 2 and 3, are also required to interpret their role in the microstructure. The following analysis explains the microstructural characteristics and formation processes of each welding region, focusing on texture, morphology, and phase formation. As illustrated in Figure 4(A), the major phase in the TIG weld zone of Super 304H stainless steel is Austenite, due to the low heat input and the high cooling rate associated with arc welding. Austenite is stable at higher temperatures, and the rapid weld-through rate of TIG welding helps maintain the phase throughout the weld region. Theoretical cooling curves for austenitic stainless steels predict that, if microsegregation localizes, even very small martensitic transformations can occur, depending on the cooling rate. The textured smoothness observed in the weld zone, however, indicates that if a transformation did occur due to the thermal cycle, the extent was insufficient to cause a significant martensitic transformation.

The dendritic shape evident in the micrograph is columnar, a form typically attributed to austenitic grains that crystallize under controlled temperature conditions. The dendritic arms are more strikingly aligned, and this observation is not misplaced, as evidenced by examples in which austenite is formed in the weld pool. The TIG welding zone exhibits a fine-grained microstructure. Such a result indicates both a low level of heat input and rapid solidification. The fracture resistance of the welded material increases as grain size decreases because smaller grains help restrict crack propagation [16]. In contrast, in the HAZ, grains tend to line out into columns and follow the direction of the heat-flow texture, improving the columnar dendritic shape that typifies the TIG-welded joint. The resulting orientation leads to improved mechanical properties, including higher tensile strength and greater fatigue resistance. TIG welding produces a dendritic structure that results from controlled, steady cooling rates. The primary dendrite arms branch perpendicular to the heat-flow direction, resulting in a more uniform texture than SMAW, which tends to exhibit irregular dendritic characteristics. The austenitic structure, which is the normal structure of the base material, Super 304H SS, may contain localized martensitic phases in

the HAZ due to steep thermal gradients and the rapid solidification conditions of TIG welding, as indicated by predictive phase diagrams. Still, close control of process parameters, especially the application of argon shielding, has limited oxidation and thermomechanical phase transformations, reduced the potential to produce a large amount of martensite, and maintained a generally austenitic structure within the weld region.



(A)

(B)

Figure 4. Welding zone microstructure: (A) Tungsten Inert Gas (TIG) welding zone, (B) Shielded Metal Arc Welding (SMAW) welding zone

Figure 4(B) shows a microstructural evaluation of SMAW welds, which demonstrates greater textural variation than other welding types. The HAZ of SMAW is highly irregular and exhibits a strong, chaotic dendritic pattern. These are the properties of SMAW because the higher heat input and slower cooling rates inherent in SMAW allow larger grains to grow. In the SMAW zone, austenite is the majority phase because Super 304H stainless steel is primarily austenitic. Austenite is likely to spread more evenly in the weld owing to the slow cooling rate associated with SMAW. However, the high heat input increases the likelihood of large-scale phase change, and in situations where cooling is inadequate or slow, ferrite may be found in isolated parts of the HAZ. Flux Coverage and the high heat provided by SMAW also ease this nucleation. Depending on the cooling rate, ferrite often forms, particularly in the HAZ, when the cooling time is sufficient for ferrite to stabilize. Although martensite formation is still possible in principle in rapid-cooling zones within the SMAW weld pool, the low cooling rate, which reflects the high heat input, reduces the likelihood of its occurrence. Instead, the retention of delta-ferrite is theoretically preferred when it is a second phase under the specific thermal dynamics of the SMAW process, thereby allowing extended exposure to elevated temperatures for compositional partitioning [18]. Microstructural observations under regulated cooling conditions indicate that, when SMAW welding is used, the microstructure of the weld region exhibits grains significantly larger than those in the TIG-welded specimen. The inverse relationship between grain size and mechanical resistance is well established: smaller grains confer greater strength and ductility. Because of its non-homogeneous nature, the SMAW process produces a grid of coarse and fine grains, which explains the preferred grain pattern in the TIG-welded microstructure. Because heat flow varies significantly across the weld section, large differences in grain shape and size result. The variable nature of heat supply and the use of flux-coated electrodes in SMAW often generate dendritic grain growth, shapes that do not exhibit as much regularity and order as in TIG welding, and inherently less consistent mechanical properties, especially tensile strength. Furthermore, slag inclusions, as byproducts of flux dispersion, can be generated in the SMAW-welded area; they can serve as crack nuclei and sites of carbide precipitation. Extended solidification, which accompanies relatively low cooling rates during SMAW welding, also facilitates large-scale phase transformations, promoting the formation of austenite as the primary solid phase in Super 304H stainless steel. This is followed by ferrite precipitation in the HAZ, which can reduce ductility and increase susceptibility to brittle intergranular failure. Finally, the elevated temperatures used during SMAW welding promote carbide precipitation at grain boundaries and further sensitize the material intergranularly. The microstructure of welded zones exhibits considerable variability in thermal history and material composition due to the welding process [19]. Although the common outcome of TIG and SMAW is an austenitic matrix, variations in heat input and cooling rate affect the formation of other potential phases, such as ferrite and martensite. These variations have been synthesized, and their influence on texture is explained in Table 4 below.

Table 4. Phase and texture comparison between Tungsten Inert Gas (TIG) and Shielded Metal Arc Welding (SMAW)

Feature	TIG Welding	SMAW Welding
Dominant Phase	Austenite	Austenite (with possible Ferrite)
Secondary Phases	Possible Martensite (minor)	Possible Ferrite and Carbide Precipitation
Texture	Smooth, regular, fine, austenitic dendrites	Irregular, coarse, ferritic, or austenitic dendrites
Formation of Ferrite	Unlikely, as cooling is rapid	Likely due to the slower cooling rate
Formation of Martensite	Unlikely (except in the heat-affected zone (HAZ) at very rapid cooling)	Unlikely, but it could form in HAZ if the cooling rate is fast enough
Phase Stability	Primarily austenitic, stable at weld temperatures	Austenitic with potential ferrite at low temperatures

3.2 Welding zone microstructure analyses after the aging process

Aging of a welded metallic alloy, especially at high temperatures, significantly affects microstructural evolution. These effects are shown in Figures 5(A) and 5(B) for stainless steel type Super 304H welded by the TIG and SMAW processes. The material stabilizes through the precipitation of carbides and other microstructural refinements after 500 h of

aging at 650 ℃. The subsequent carbide dispersion along grain boundaries and in the matrix controls the weld strength, ductility, and susceptibility to sensitization. Aging of a TIG-welded specimen at 650 ℃ in Figure 5(A) shows no structural differences, i.e., the same characteristics as before heat treatment; the microstructure remains a face-centered cubic (FCC) austenite matrix. However, an exact analysis of the interface region in Figure 6(A) reveals carbide formation that favors austenite grain boundaries. This effect implies that carbon segregation and nucleation on the dissimilar surfaces around austenite-austenite interfaces occur more rapidly during aging, limiting the distribution of carbides within the grains. As such, deleterious chromium carbides (e.g., $Cr_{23}C_6$ or Cr_7C_3) precipitate near the grain periphery. The aged specimen has a coarse boundary morphology, distinct evidence of disrupting the homogeneity of the initial texture relative to the as-welded microstructure, and a reorganized dendrite structure. The boundaries produced by dendrites are now much sharper and in a position to promote the precipitation of carbides. The high aging temperature of 650 ℃ greatly promotes sensitization, i.e., the formation of chromium carbides at these boundaries, thereby increasing the microstructural susceptibility to intergranular sensitization. Ductility degrades and is, in fact, abetted by accumulated carbides, which can cause brittle fracture. SMAW in Figure 5(B) shows grain boundary precipitation of carbides, similar to that found in the TIG specimen, but the texture is much more heterogeneous. SMAW microstructure is naturally coarser and more irregular, and it becomes even coarser during aging, indicating stronger carbide banding around grain boundaries [20]. However, austenite FCC remains the major phase, and aging once more leads to the precipitation of carbides at grain boundaries. Unlike the TIG microstructure, there may also be ferrite (body-centered cubic (BCC)), especially in parts with a slower cooling rate, and carbides more readily attack these ferritic areas since they have less solubility for carbon. In both SMAW and TIG, the precipitates are chromium carbides on the grain boundaries, but in SMAW, the grain size is larger. Therefore, the distribution of these carbides is less homogeneous. The formation of carbides in the SMAW joint is more prevalent than in the TIG joint, due to the lower cooling rates in the SMAW process.

Ferrite could also form in the SMAW weld, leading to larger carbide precipitates and making some areas prone to intergranular cracking. Irreversible grain structure and slag inclusions in the SMAW specimen also cause greater non-uniformity of carbides, thus creating uneven mechanical properties in the most heavily processed areas. The comparison of the evolution of the metallurgy of TIG and SMAW weldments after annealing at 650 ℃ at 500-hour intervals reveals significant deviations in carbide precipitation characteristics. Such observations can be explained by differences in cooling-rate contours and microstructural changes between the two welding methods. Table 5 below summarizes these key differences.



(A) (B)

Figure 5. Welding zone microstructure after 500 h aging at 650 ℃: (A) Tungsten Inert Gas (TIG) welding zone, (B) Shielded Metal Arc Welding (SMAW) welding zone

Table 5. Key differences between Tungsten Inert Gas (TIG) and Shielded Metal Arc Welding (SMAW) after aging

Aspect	TIG Welding (Aged at 650 ℃)	SMAW Welding (Aged at 650 ℃)
Microstructure	Fine-grained, uniform, but with visible grain boundary precipitation	Coarse-grained, irregular, with more extensive carbide precipitation
Phase Composition	Predominantly austenite with minor carbide formation	Predominantly austenite, with possible ferrite and carbide formation
Carbide Precipitation	Carbides form along austenitic grain boundaries, with minimal in the matrix	Extensive carbide precipitation along grain boundaries, especially in ferritic regions
Texture	Fine dendritic structure with disrupted grain boundaries	Coarse dendritic structure with non-uniform carbide distribution
Effect on Ductility	Reduction in ductility due to grain boundary carbide formation	More pronounced decrease in ductility, with risk of intergranular cracking
Effect on Sensitization Susceptibility	Potential for intergranular sensitization due to carbide formation	Higher risk of intergranular sensitization, especially in ferritic regions

The authors explained the differences in carbide precipitation processes in TIG- and SMAW-welded joints

after aging, which were due to the differing heat inputs. Due to the relatively low heat input and high cooling rate, TIG welding produces a finer microstructure and enables more rational carbide precipitation. In SMAW welding, the cooling rate is slower, allowing high-rate carbide precipitation, especially in ferritic zones, which are naturally prone to carbide formation [21]. In addition, TIG welding typically has a fine, homogeneous microstructure, promoting a uniform distribution of carbides. Still, SMAW welding has a coarse structure that allows ferrite to form and has an inhomogeneous distribution of carbides. The flux used in SMAW introduces impurities and further decreases the cooling rate, resulting in a more heterogeneous microstructure. TIG welding is more controlled; therefore, there is less variation in cooling rates, resulting in a more homogeneous carbide distribution.

3.3 Welding zone microstructure scanning electron microscopy, energy-dispersive X-ray spectroscopy, and transmission electron microscopy analyses after the aging process

The two SEM images in Figures 6(A) and (B) below, given in the present case, exemplify the morphology of the welding zone subjected to a 650 ℃ holding temperature over 500 hours, where the welding area has two welding processes: (a) TIG and (b) SMAW. The TIG weld zone (shown in Figure 6(A)) is fine-grained, austenitic, and homogeneous. Figure 6(B) shows the SMAW weld zone, which exhibits a rough, irregular texture due to lower cooling rates and higher heat input. Both weld zones exhibit some carbide precipitation along grain boundaries, particularly chromium carbides (M23C6), due to the high-temperature aging treatment. These morphological differences have a crucial effect on the material's mechanical properties and susceptibility to sensitization, which is why the cooling rate and heat input during welding are important. The SEM image of the TIG weld zone in Figure 6(A) shows a fine-grained, austenitic microstructure. The relatively slow heating in the controlled heat stage of the TIG process is attributed to the dendritic pattern. Dendritic solidification involves the formation of primary dendrites (trunks) and secondary dendrites (branches), in which the liquid metal forms tree-like structures. This tendency is common in austenitic stainless steel because it crystallizes in the FCC phase and has high-temperature stability. Columnar dendrite refers to a steady flow of cooling velocity and grain growth in the direction of heat flow during the process.

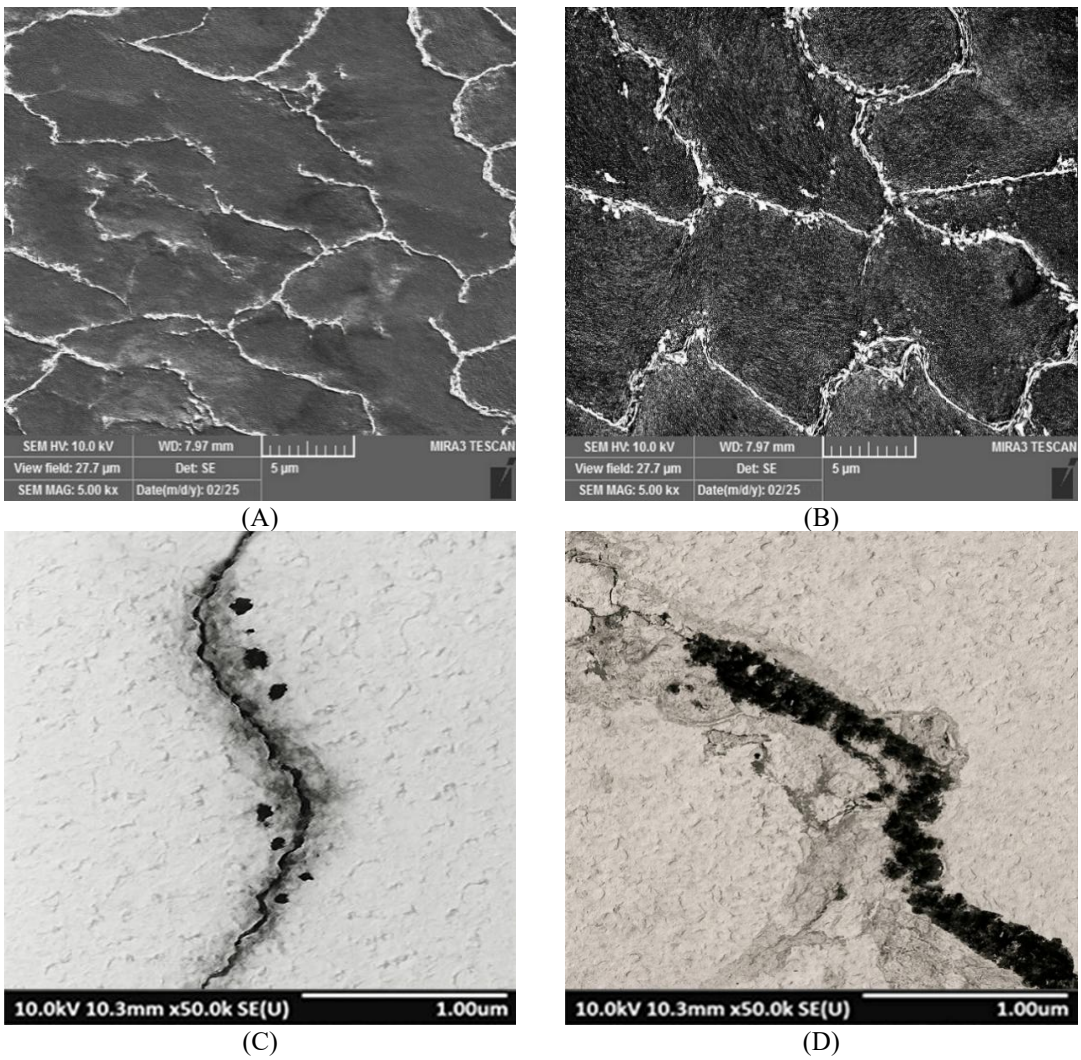


Figure 6. Welding zone scanning electron microscopy (SEM) and transmission electron microscopy (TEM) after 500 h aging at 650 ℃: (A) Tungsten Inert Gas (TIG) welding zone SEM, (B) Shielded Metal Arc Welding (SMAW) welding zone SEM, (C) TIG welding zone grain boundary TEM, (D) SMAW welding zone grain boundary TEM

Table 6. Tungsten Inert Gas (TIG) vs. Shielded Metal Arc Welding (SMAW) post-aging effects comparison

Aspect	TIG Welding (Aged at 650 °C)	SMAW Welding (Aged at 650 °C)
Grain Size	Fine and uniform	Coarse and irregular
Dendritic Structure	Smooth, regular	Irregular and coarse
Carbide Precipitation	Controlled along grain boundaries	Extensive, more in ferritic regions
Secondary Phases	Minor martensite (heat-affected zone (HAZ))	Ferrite and carbide precipitates
Phase Composition	Predominantly austenite	Predominantly austenite with ferrite possible
Ductility	Moderate decrease due to carbide formation	Significant reduction due to carbide formation in ferritic regions
Toughness and Fatigue Resistance	Higher, due to fine-grained structure	Lower, due to coarse grains and carbide distribution

Table 7. Energy-dispersive X-ray spectroscopy (EDS) results for Tungsten Inert Gas (TIG) and Shielded Metal Arc Welding (SMAW) joints after aging treatment

Point No.		1	2	3	4	5	6	7
Elements wt.%	Nb	48.18	47.76	53.92	55.06	61.12	-------	-------
	Cr	24.8	23.89	24.83	23.64	17.11	43.31	75.14
	Fe	18.81	20.74	16.26	18.46	19.13	50.74	19.79
	Mo	5.42	4.97	3.25	1.42	1.21	2.42	0.76
	Mn	2.21	1.82	1.31	1.21	1.02	3.11	4.02
	Ni	0.58	0.82	0.43	0.21	0.41	0.42	0.29

This is typically coupled with better mechanical properties, including higher strength and fatigue resistance. The tiny grain size impedes crack development, thereby boosting toughness. M23C6 carbide precipitation at the grain boundary requires a heat treatment of 650 °C. Chromium from the austenitic matrix migrates to the interfaces. Consequently, the carbon remaining near it is depleted during this process, making the material more susceptible to intergranular sensitization [22]. The controlled heat input and fast cooling rates during TIG welding result in an equiaxed distribution of the fine carbides in the exposure region, which is a more desirable microstructure for retaining resistance to intergranular sensitization. However, grain boundary carbide precipitation may reduce ductility. Low-temperature exposure may also cause carbide growth, reducing tensile strength and impact toughness. Despite its ability to impart carbide precipitation effects on long-term, high-temperature strength, the low-grained microstructure retains respectable fracture toughness.

Figure 6(B) depicts the SMAW weld zone with a coarser, more irregular dendritic morphology due to the higher heat input and slower cooling rate of the SMAW process. Due to nonuniform heat during solidification, the resulting dendritic structure is less organized than that obtained in the TIG test sample. The discontinuous microstructure adversely affects the secondary phases, making the material more vulnerable to crack propagation under stress. The dominant dwell time at high temperatures also facilitates the development of large grains, reducing grain boundary strengthening, decreasing ductility, and restricting fracture toughness. An increase in the population of carbides that tend to form along the grain boundaries, including a relatively high proportion of M23C6 precipitates, also helps strengthen the grain boundaries against embrittlement. Large carbide shops, especially those found in ferritic (BCC) areas, are known to cause localized hardening and high intergranular susceptibility to cracking. The slow-cooling regime in SMAW welds also causes austenite to transform into ferrite, particularly in regions with slower cooling rates. In ferrite, carbide is expected to precipitate strongly at high temperatures, and heterogeneous carbide distribution is a major microstructural feature that contributes to susceptibility to intergranular sensitization. Moreover, ferrite precipitation reduces the weld's impact toughness, as shown in the toughness test data [23].

A substantial amount of carbide precipitation in structural steels preferentially occurs at grain boundaries. In cases where fine grains and high quenching rates can be favored by experimental arrangements of metallurgical processing conditions, as is frequently the case with high-strength steels, a beneficial result can be achieved on two counts simultaneously: high tensile strength and high impact toughness may both be retained. In comparison, alloys that undergo rapid quenching rates and large grain sizes, as found in thick-section steels, exhibit an increased concentration of carbide nucleation in the ferritic areas, leading to uneven precipitation, variability in mechanical properties, reduced ductility, and increased exposure to intergranular areas prone to brittle fracture. A major factor affecting carbide precipitation is the welding process. With high-speed TIG welding, high-temperature phase transformations are limited due to the rapid cooling rate. This fine-grained, highly homogeneous austenitic matrix gives superior mechanical properties to the TIG-welded joints and prevents the formation of massive secondary phases during initial solidification.

On the other hand, the welding processes in the SMAW family have a slightly slower cooling rate, which allows local ferrite nucleation; the austenite-ferrite transformation occurs faster than the secondary carbide precipitation reaction, causing sensitization of metals. In SMAW welds, a continuous network of large carbides is observed across grain boundaries and in ferritic areas, which are known to cause localized depletion of chromium and increase susceptibility to localized intergranular sensitization. However, TIG and SMAW welds remain carbide-precipitate-free at grain boundaries, producing a fine, homogeneous microstructure typical of high-speed TIG welding [24]. Table 6 compares the post-aging effects of both investigated welding processes.

The presence of niobium in the EDS results shown in Table 7 suggests that the Nb-rich precipitates remained dominant in the TIG-welded joint, consistent with typical alloy behavior, Ni Carbide. The precipitates were continuous Nb-carbide precipitates at the grain boundaries, as marked by white dotted rectangles 1 and 2, though they were not yet a fully developed precipitate network. More specifically, at these boundaries, EDS identified two distinct second phases, demarcated by the

white dotted rectangles 3 and 4 in Figure 6(A). Figure 6(A) illustrates this phenomenon at high magnification. The bright and the dark second phases were analyzed using the EDS points (points 3 and 4). Data indicated a large concentration of Nb in the radiant second phase and a high concentration of Cr in the dark second phase. As a result, both major Nb-carbide precipitates and Cr-enriched carbide precipitates remained on grain boundaries even after 500 hours of aging. In contrast, the Cr-carbide dissolved rapidly along grain boundaries, and the two precipitate types were evenly distributed throughout the structure's grain boundaries. Figure 6(B) for the SMAW joint indicates a substantial increase in the density of Cr-rich precipitates on grain boundaries, with a corresponding change in morphology to chain-like arrays extending across them. At the same time, the grain boundary width is much broader, which means that the precipitates have filled nearly all of the interfacial volume. EDS analysis showed that these particles were highly Nb-rich, suggesting they are still Nb-containing precipitates. There is clearly a higher incidence of intergranular precipitate coarsening during this time, with a conspicuous increase in the number and size of the precipitates, as marked at points 5, 6, and 7. These precipitates now completely cover the grain boundaries, forming a continuous network across them. The EDS results also indicated a high concentration of chromium in these intergranular precipitates, consistent with the formation of Cr-rich carbides (typically M23C6 in Super 304H aged at a suitable temperature) [25].

Figures 6(C) and (D) show TEM images of the aged samples from the SMAW and TIG weld microstructures at the grain boundary. These correspond to retrieved samples of the weld metal. In the TIG sample (Figure 6(C)), large granular precipitates are observed. These grains were characterized as the main Nb carbides in the above analysis. The grain boundaries are quite narrow, and a small distance from the precipitates (also Nb carbides) has been shown to exist near the boundaries. However, the Cr carbide precipitated on the grain boundary is smaller than that precipitated on the SMAW grain boundary. Besides, the smaller second form of carbide began to appear at grain boundaries. A previous EDS examination revealed that the large carbides in the intragranular domain were secondary Nb carbides, and their identity was confirmed as NbC by SAED. Figure 6(D) illustrates large intergranular carbides precipitated on the grain boundary, which contained high Cr and minimal or no Nb in much darker zones on the grain boundary; the identity was M23C6 carbide, as determined by SAED. The Cr-bearing carbides were relatively scattered along grain boundaries due to the large number of Cr-rich carbides, the high heat input in SMAW, and the long aging time. The extent of precipitate formation along grain boundaries was very great, especially on the grain boundaries. There was greater coarsening of the precipitates in SMAW than in TIG, nearly covering the grain boundaries [26].

The SAED patterns of TIG- and SMAW-welded joints show precipitates at grain boundaries. Based on the results in Figure 7(A), a discontinuous distribution was observed at point 1 in the TEM picture in Figure 6(C), as a small quantity of carbides was distributed along grain boundaries. Based on the above analysis and EDS results, it can be concluded that M23C6 carbides were discontinuously precipitated at the grain boundaries after 500 h of aging. The precipitate at point 2 was massive and irregularly sized, and it was present both within grains as small secondary-phase islands and on grain boundaries. EDS analysis revealed that it contained significant Nb and was also identified as NbC by SAED in Figure 7(B). The SAED pattern of the bright secondary phase was indexed to the [011] zone axis, and the measured d-spacings were 2.58 Å, 2.23 Å, and 1.58 Å, consistent with the FCC structure of NbC. Likewise, from the dark outgrowths at the grain boundaries, the d-spacings were measured at 2.37 Å and 2.16 Å along the same zone axis [111], thus unambiguously assigning them to the M23C6 phase.

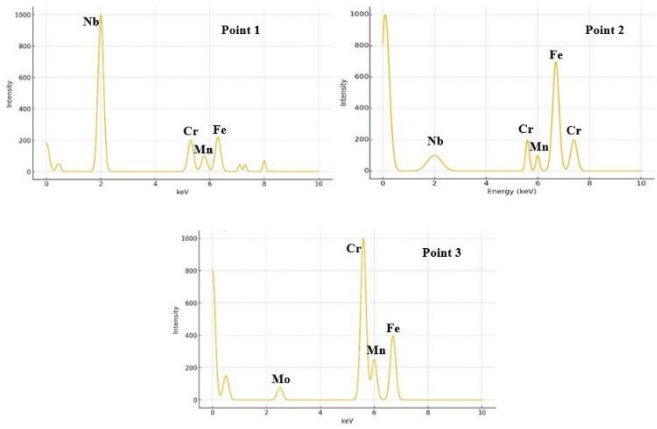


Figure 7. (A) and (B) Tungsten Inert Gas (TIG) selected area electron diffraction (SAED), (C) Shielded Metal Arc Welding (SMAW) SAED

SMAW TEM reveals precipitates with a continuous distribution along grain boundaries, and the degree of coarsening was also increased. EDS results indicated that they consisted of Cr, Fe, and Mo, which were identified as M23C6 based on the SAED pattern in Figure 7(C) (point 3 in Figure 6(D)). It is well known that sigma phase is a very brittle intermetallic phase that typically occurs in austenitic stainless steel weld metal [27, 28], and high temperatures can also promote its formation [29]. In this work, results at 650 °C show no σ-phase formation; thus, σ-phase precipitation is expected at higher aging temperatures.

3.4 Toughness test results analysis

Figure 8(A) of the TIG welding joint impact test shows a ductile fracture with a distinctive fibrous appearance. The fracture surface exhibits a small-scale fibrous structure characteristic of ductile fractures, in which the indent material undergoes high plasticity before failure. The fibrous microstructure is most likely explained by microvoid coalescence, i.e., the formation of small pores within the material and their coalescence into larger ones that eventually lead to fracture, as observed in materials with higher elongation, as seen here in metals. Fine texture is also associated with a noble microstructure within the TIG-welded joint. The heat applied by TIG welding is better controlled, resulting in a faster cooling rate and smaller grain sizes in the weld zone and HAZ. This grain-structure fineness is associated with increased resistance to crack propagation and, consequently, higher material toughness in its initial aging stages. As the carbides age, however, the microstructure is altered by their precipitation, as described below. The morphological difference shown in Figure 8(B) is due to unequal plastic deformation during solidification in metallurgical mechanics. The microvoids are becoming more

prominent, and the grain texture is coarser in the SMAW specimen than in the TIG specimen. The occurrence of these holes is associated with ductile fracture conditions, which involve the breaking of grain boundaries or precipitate interfaces. Localized failures result from the coalescence of microvoids, meaning that the steel has deflected sufficiently for the voids to nucleate and grow. The deeper holes in the SMAW weld support the conclusion that there was significantly greater plastic deformation in the steel than in the TIG weld [30].

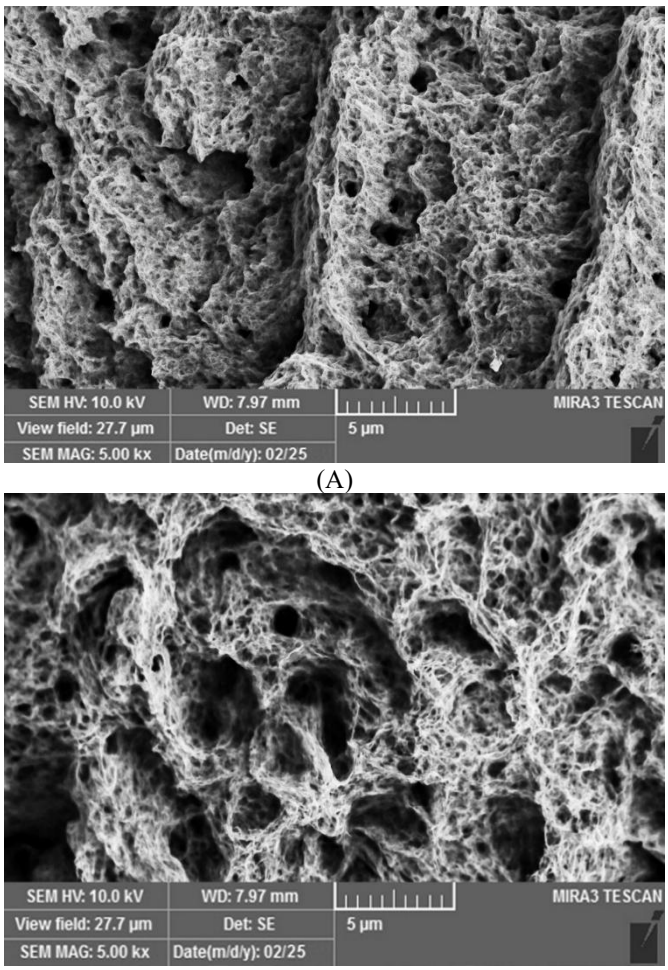


Figure 8. Impact test fracture scanning electron microscopy (SEM): (A) Tungsten Inert Gas (TIG) welding joint, (B) Shielded Metal Arc Welding (SMAW) joint

The extrapolation of this discrepancy is the significantly higher heat input and resulting slower cooling rate inherent in the SMAW process, which allows extended time at elevated temperatures, favoring the development of larger, more brittle microstructural constituents in the HAZ. SMAW microstructure exhibits an unequal grain-size distribution and dimensions that can be said to be coarser, thus creating an irregular strain field that facilitates the formation of microvoids, which are highly pronounced but poorly distributed. The presence of MX carbides, which occur as primary carbides in long-aged Super 304H steel, is a prevailing cause of toughness loss. At 650 °C, such carbides nucleate and grow in the microstructure after 500 h. These carbides lock in dislocations during the early stages of aging, thereby strengthening the material. In older ages, though, they grow, become hard and brittle, and act as stress concentrators. Such microstructural changes predispose the material to crack initiation at the carbide-matrix boundaries, thereby reducing overall toughness. It is clearly obvious that the formation of the MX carbides embrittles the TIG and SMAW weld zones, as evidenced by the fracture surfaces, and the noted reductions in the toughness of the steel from 213 ± 4 J/cm² before welding to 183 ± 4 J/cm² following an initial TIG weld, and from 198 ± 4 J/cm^2 before welding to 158 ± 4 J/cm^2 after an initial SMAW weld. In addition, the coarsening carbides disrupt the matrix's continuity, reducing the material's capacity to absorb impact energy. As a result, impact toughness decreases with aging. In addition, the large carbides also limit plastic deformation under impact loading. They would encourage brittle fracture behavior, as observed on the fracture surfaces of both TIG and SMAW welds [31].

Aging Super 304H stainless steel at 650 °C for 500 hours induces significant microstructural changes, particularly in the BM and the welded region, which eventually deteriorate fracture toughness. In such treatment, MX carbide nucleation occurs along grain boundaries and in the matrix; when they attain a coarse size, they lead to embrittlement. This leads to microstructural discontinuities that reduce a material's ductility under applied stress. The heavy precipitates weaken the weld zone under aged conditions, affecting both TIG and SMAW joints. Fracture surfaces, as revealed by SEM, show brittle carbide phases that increase in abundance with aging time. At the same time, the plasticity of steel, which measures its ability to absorb energy from impact loads, decreases because large precipitates constrain deformation. The fracture character observed throughout the alloy, with larger pores in SMAW and more stringy textures in TIG, indicates reduced toughness, as evidenced by increased brittleness [32]. The TIG welding technique also employs a controlled heat-input regime and generally produces a finer-grained microstructure in both the weld metal and the HAZ. This microstructural fineness prevents the coarse carbide precipitation usually resulting from post-weld aging, thereby reducing the concomitant loss of joint toughness. The comparatively high cooling rates of TIG welding improve the microstructure and, in turn, resistance to crack initiation and propagation. The TIG joint has an initial toughness of 213 ± 4 J/cm^2, which decreases only slightly to 183 ± 4 J/cm^2 after 500 h of thermal aging at 650 °C, indicating minimal degradation due to carbide precipitation. (SMAW) On the other hand, it has high heat intensity and a fast cooling rate, resulting in a coarser microstructure in both the weld and the HAZ. This violent structure makes it prone to brittle failures due to the activation of larger carbide precipitates. In addition to the vulnerability to carbide-induced embrittlement, rapid cooling introduces increased residual stresses. Following 500 hours of thermal aging, the SMAW weld joint had a significant decrease in toughness from the 198 ± 4 J/cm^2 base value to 158 ± 4 J/cm^2, a 20.2% decrease. This dramatic reduction is thought to be due to intensive carbide nucleation and additional evolution of residual stresses, while the TIG joint was also reduced by 14.1% under the same conditions.

Through a comparative analysis of Super 304H stainless steel TIG- and SMAW-welded specimens, pronounced differences in fracture behavior, microstructural alterations, and reduced impact toughness are observed. When the welded joints experience ductile failure, the TIG weld exhibits a finer, more homogeneous microstructure, indicating lower toughness attenuation than the SMAW joint, which has a coarser grain size and a strong tendency toward void

formation. The precipitation of carbides is a phenomenon resulting from aging treatment, leading to general embrittlement of the respective weld zones. In TIG welding, the ensuing decline is less pronounced due to faster cooling rates and relatively lower residual tensile stresses [33]. Table 8 below systematically summarizes the effect of each welding technique on material performance over time.

Table 8. Tungsten Inert Gas (TIG) and Shielded Metal Arc Welding (SMAW) welded joints after aging, impact fracture, and scanning electron microscopy (SEM) comparison

Feature	TIG Weld	SMAW Weld
Fracture Type	Ductile fracture with fine, fibrous texture.	Ductile fracture with larger voids and coarser texture.
Texture	Fine, fibrous, indicating plastic deformation before fracture.	Coarser texture, indicating more significant plastic deformation and larger void formation.
Voids	Fewer and smaller voids, indicating less deformation.	Larger and more numerous voids indicate greater plastic deformation.
Fracture Surface	Smooth fibrous surface with microvoids.	Larger voids and more pronounced crack paths.
Cooling Rate Impact	Controlled heat input and faster cooling lead to a finer microstructure and less carbide formation.	A slower cooling rate resulting from high heat input leads to a coarser microstructure and larger carbide precipitates.
Carbide Effects on Toughness	Carbides form but with less coarsening, resulting in moderate degradation of toughness.	Coarse carbide precipitates cause significant embrittlement and lower toughness.
Impact Toughness After Aging	Decreases from 213 J/cm² to 183 J/cm² (14.1% reduction).	Decreases from 198 J/cm² to 158 J/cm² (20.2% reduction).
Carbide Precipitation	Carbides are present but remain relatively small and dispersed, resulting in moderate embrittlement.	Carbides are larger and more concentrated, leading to a more brittle fracture.
Microstructure	Fine-grained microstructure with controlled carbide formation.	Coarse-grained microstructure with large carbide precipitates and residual stresses.
Plastic Deformation	Less extensive, with finer texture and smaller voids.	More extensive, with larger voids and more significant deformation.
Welding Technology Impact	TIG welding results in a finer microstructure and less degradation in toughness over aging.	SMAW welding leads to a coarser microstructure and a greater loss of toughness due to slower cooling and higher residual stresses.
Overall Toughness	Moderate degradation in toughness (183 J/cm² after aging).	Significant degradation in toughness (158 J/cm² after aging).

3.5 Vickers microhardness results analysis

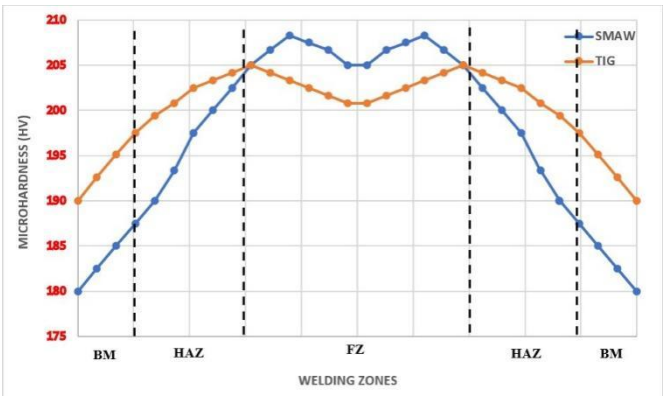


Figure 9. Aged welding joints' microhardness test results

The current study tested the microhardness of Super 304H SS BM, weld joints, aged, and HAZ at 650 °C after 500 h. The joints were produced using SMAW and TIG welding techniques; the microhardness results for the two joints are shown in Figure 9, with the corresponding BM hardness (about 190 HV) for both samples. In the HAZ, TIG-deposited material exhibited the highest hardness (205 HV) at the fusion line, which decreased toward the FZ. This hardness distribution is characteristic of a finely grained, uniformly dispersed carbide precipitate. Conversely, the hardness was less variable in the TIG-welded HAZ than in the SMAW (200 HV), which can be attributed to the relatively high heat input and slower cooling rate. In the FZ, TIG exhibited the maximum hardness of 202 HV, with a gradual reduction in hardness attributable to a compositionally uniform austenitic structure that solidified freely. SMAW joint fusion line was observed (~205 HV) due to the elevated input, which induced larger and non-homogeneous grains and an intermediate hardness compared to that of TIG welds.

The major difference between the welding processes SMAW and TIG lies in their heat inputs and opposing cooling curves. The parameters have a vast impact on the microstructure, hardness, and mechanical performance of welded joints. The flux-covered electrode in SMAW also provides more heat than the pure tungsten electrode in TIG. Much slower cooling rates accompany the high heat input of SMAW during weld-pool solidification and post-solidification.

This extended cooling allows grain coarsening and the precipitation of secondary phases, especially carbonitrides, and favors the formation of a dendritic structure. This enhanced heat input, coupled with prolonged cooling, results in significantly coarse grains in the HAZ and even in the FZ. These larger grains compromise the material's ductility, increasing the tendency toward brittle failure. The coarsening effect is very pronounced in the HAZ and FZ, resulting in greater variation in the microhardness curves across the weld cross-section. Moreover, slower cooling facilitates the abundant precipitation of chromium carbides (M23C6) along grain boundaries. These carbide precipitates hinder the counter-movement of dislocations, consequently increasing the hardness of both the HAZ and the FZ. However, a high volume fraction of intergranular precipitates also renders it brittle and significantly enhances microstructural susceptibility to sensitization at higher exposure temperatures, such as 650 °C. This problem is further exacerbated by the co-location of large carbides and ferrite in the SMAW microstructure, resulting in an uneven distribution of

mechanical properties throughout the joint [34].

Unlike SMAW, TIG welding produces much less heat input. This difference is achieved using a stationary tungsten electrode with argon as the shielding gas, under precise control. The reduced heat input accelerates the cooling rate during solidification, causing the temperature variation to occur much faster than in SMAW—the microstructures in the HAZ and the FZ exhibit significantly smaller grain-size distributions. The close grain spacing, in turn, favors enhanced mechanical strength and elongation. The microhardness values are more consistent across all weld zones due to the uniform distribution of phases, especially austenite, and the limited extent of carbide precipitation. Although dendritic carbides can be detected in a TIG-welded joint, the low heat input and high cooling rate hinder their coarsening and dispersal. Instead, they are smaller and more evenly distributed, especially along austenite grain boundaries. The corresponding tendency is explained by high cooling rates, under which large quantities of carbides and/or ferrites are not formed, and, consequently, the overall toughness and ductility of the material are not compromised. The TIG process, therefore, produces less variation in hardness values across the BM, HAZ, and FZ than SMAW.

The microhardness results indicate that heat treatment at 650 ℃ leads to the precipitation of carbides, especially chromium carbide (M23C6), that occurs predominantly at grain boundaries. Precipitation occurs in boundary sites through carbon diffusion and chromium segregation. The tertiary forms, which develop during the process, alter mechanical properties such as hardness, ductility, and tensile strength. The microstructure of the TIG weld is fine-grained; hence, the precipitating carbides are small and located along austenite grain boundaries. The condition results in a moderate increase in hardness over the HAZ and the FZ. Regardless of the hardening, the fine-grained microstructure and the uniform distribution of carbides in the TIG-welded joint are associated with reduced embrittlement, so the resulting loss of toughness is minimal after 500 hours of aging. The moderately low effect of the precipitated carbide on the mechanical performance of the TIG joints is largely due to the small, uniformly distributed carbides that maintain ductility [35]. In contrast, SMAW welds have a coarse-grained microstructure, with larger carbide particles, leading to increased embrittlement. Bigger carbides, especially those in ferritic regions, increase stress concentrations and promote intergranular cracking. Accordingly, empirical research shows that TIG-welded joints exhibit a slight increase in microhardness, particularly in the HAZ and FZ. Enhancements in such hardness are attributed to carbide precipitation, which occurs during consecutive aging. However, TIG welding has a finer grain size and a more uniform carbide distribution, resulting in a more stable hardness profile and better overall hardness for the joint than the SMAW joint. The HAZ of TIG welds has a noticeable hardness peak. Still, the magnitude of the hardness difference is relatively small due to the high-quality microstructure and carefully controlled carbide nucleation. On the other hand, the SMAW joints with coarser grains and a high degree of carbide development exhibit significant changes in hardness following aging. The FZ and HAZ hardness values increase significantly, driven by the larger size of the carbides. However, the weld is also embrittled. The unbalanced carbides in SMAW also create large hardness gradients in the weld areas, thus providing less consistent hardness values in the joint [36].

Table 9. Microhardness and microstructural characteristics comparison between Tungsten Inert Gas (TIG) and Shielded Metal Arc Welding (SMAW) welded joints after aging at 650 ℃

Aspect	TIG Welding	SMAW Welding
Microstructure	Fine, homogeneous microstructure	Coarse, irregular microstructure
Heat Input	Low heat input	High heat input
Cooling Rate	Fast cooling rate	Slow cooling rate
Grain Structure	Fine-grained structure	Coarse-grained structure
Carbide Precipitation	Controlled carbide precipitation	Extensive carbide precipitation
Carbide Size	Small, dispersed carbides	Large carbides
Carbide Distribution	Uniform carbide distribution	Non-uniform carbide distribution
Phase Composition	Predominantly austenite	Predominantly austenite, with ferrite possible
Hardness in BM	Stable around 190 HV	Stable around 190 HV
Hardness in HAZ	Peaks around 205 HV, then almost stable in FZ	Increased to 205 HV, then increased in FZ
Hardness in FZ	Drop to around 201 HV at the center	Drop to around 205 HV at the center
Hardness Variation	Less variation across BM, HAZ, and FZ	Significant variation across BM, HAZ, and FZ

Note: fusion zone (FZ), heat-affected zone (HAZ), base metal (BM).

The microhardness values for TIG- and SMAW-welded samples are given in Table 9 for comparison. This table specifically examines microstructure, cooling rate, carbide behavior, hardness distribution, and the effect of aging treatment. The main conclusion is that TIG welding yields a uniform microstructure, i.e., the hardness variation throughout the joint is relatively constant. In contrast, SMAW welding exhibits a wide variation in hardness due to coarser grains and a non-uniform distribution of carbides.

4. CONCLUSIONS

The current study aims to review the effect of two welding techniques: TIG and SMAW, on the microstructural transformation, mechanical properties, and inferred sensitization susceptibility of Super 304H stainless steel. These findings conclusively reveal that welding parameters influence weld zone characteristics. These results are essential for understanding the long-term performance of welded stainless steel at high temperatures. In the conclusions, the main observations are summarized, and the material behavior between the two welding methods after aging is highlighted.

A. TIG welding gives fine control over heat and causes hastened cooling of the welding aftershocks, thus creating a smooth and fine-polished microstructure. In comparison, SMAW welding results in significant heat nugget formation and prolonged cooling, thereby producing an inhomogeneous, Coarse microstructure. Carbide precipitation began at 650 ℃ after 500 hours of aging in both welding techniques, with

M23C6 carbides forming almost exclusively along grain boundaries. Notably, the SMAW-welded specimen exhibits greater brittleness, as evidenced by increased cracking.

B. For both the TIG joint and SMAW Joint, aging resulted in a loss in toughness, although aging was quite significant in the SMAW welds. These TIG-welded specimens showed a 14.1% decrease in impact toughness (from 213 J/cm² to 183 J/cm²). At the same time, the SMAW-welded samples were reduced from 198 J/cm² to 158 J/cm², a drastic decrease exceeding the 9.9% drop observed in the welded samples. The significant difference certainly shows the increased embrittlement that can be found in the case of the SMAW process. Microhardness measurements showed that the hardness profile was more uniform across the BM, HAZ, and FZ in the TIG-welded joints, with a maximum of 205 HV in the HAZ. In SMAW-welded joints, the variations were significant, with larger, irregular carbide precipitates, resulting in a heterogeneous hardness contour.

C. The current analysis shows that microstructural change through precipitation is one of the major factors in the loss of grain-boundary toughness in TIG and SMAW procedures. The volume fraction of the precipitates is the same under all conditions; however, TIG specimens have a homogeneous, less dispersed distribution of precipitates, whereas SMAW specimens have a more concentrated distribution of larger aggregates. Such structural dissimilarity culminates in mechanical disparities, where the TIG-welded, finer-grained final products are less susceptible to intergranular cracking and exhibit less ductility degradation than SMAW welds, whose counterparts are coarser-grained and exhibit greater resistance to fracture. The TIG process, therefore, provides higher tensile and fatigue strengths, whereas the SMAW process, due to its gradual cooling, allows lower impact strength and elongation.

D. This paper has shown that to know if the intergranular precipitation can sensitize a material, the spatial distribution and the size of the precipitates are important characteristics of the precipitates. TIG welding under thermal arc conditions yields a uniform precipitate structure with small particles, whereas manual SMAW welding results in a heterogeneous precipitate structure with comparatively large particles. Based on microstructural investigations, it can be concluded that carbide nucleation in TIG-welded joints is controlled and uniform after aging at 650 ℃, compared to SMAW-welded joints; thus, they are less likely to be sensitized and intergranularly degraded.

E. The records also state that the nonhomogeneous composition following SMAW welding undermines the material's longevity, especially in a high-temperature environment. On the other hand, TIG welding has a favorable thermal profile, as its predetermined low-discrete heat and refined grain size provide high thermal stability under long-term exposure to high temperatures.

REFERENCES

[1] Purzyńska, H., Golański, G., Sroka, M., Sasiela, A., Zieliński, A. (2024). Microstructure characterization and mechanical properties of austenitic Super 304H steel after operation. International Journal of Pressure Vessels and Piping, 211: 105294. https://doi.org/10.1016/j.ijpvp.2024.105294

[2] Wu, Y., Chai, F., Liu, J.J., Wang, J.Q., Li, Y., Du, C.C. (2024). Strengthening and embrittlement mechanisms of Super 304H steel during long-term aging at 650 °C. Materials, 17(3): 740. https://doi.org/10.3390/ma17030740

[3] Zieliński, A., Wersta, R., Sroka, M. (2022). The study of the evolution of the microstructure and creep properties of Super 304H austenitic stainless steel after aging for up to 50,000 h. Archives of Civil and Mechanical Engineering. 22: 89. https://doi.org/10.1007/s43452-022-00408-6

[4] Xiao, X.P., Li, D.Z., Li, Y.Y., Lu, S.P. (2022). Effect of Nb on the microstructural evolution and microhardness of Super 304H austenitic stainless steel weld metals during long-term aging. International Journal of Materials Research, 113(1): 33-43. https://doi.org/10.1515/ijmr-2021-8263

[5] Li, Y., Wang, X. (2021). Precipitation behavior in boundaries and its influence on impact toughness in 22Cr25Ni3W3CuCoNbN steel during short-term ageing. Materials Science and Engineering: A, 809: 140924. https://doi.org/10.1016/j.msea.2021.140924

[6] Zhao, L., Li, X.Y., Xu, L.Y., Han, Y.D., Hao, K.D., Zheng, X.F. (2024). Effect of microstructure evolution on mechanical properties and oxidation behavior of Super 304H and HR3C after long-term service. Journal of Materials Science, 59: 22206-22227. https://doi.org/10.1007/s10853-024-10230-5

[7] Tikhonova, M., Belyakov, A., Kaibyshev, R. (2023). Effect of aging on secondary phases and properties of an Super 304H austenitic stainless steel. Materials Science and Engineering: A, 877: 145187. https://doi.org/10.1016/j.msea.2023.145187

[8] Xiao, X.P., Li, D.Z., Li, Y.Y., Lu, S.P. (2021). Intergranular precipitation behavior and its influence on the stress relaxation cracking susceptibility of Super 304H austenitic stainless steel weld metal during long-term aging. Materials Characterization, 178: 111309. https://doi.org/10.1016/j.matchar.2021.111309

[9] Jin, X., Xia, X.X., Li, Y.F., Zhao, Y.F., Xue, F., Zhang, G.D. (2019). Quantitative study of microstructure evolution and the effect on the mechanical properties of Super304H during aging. Materials at High Temperatures, 36(5): 459-470. https://doi.org/10.1080/09603409.2019.1632508

[10] Dash, M.K., Karthikeyan, T., Mythili, R., Vijayanand, V.D., Saroja, S. (2017). Effect of long-term thermal exposures on microstructure and impression creep in 304HCu grade austenitic stainless steel. Metallurgical and Materials Transactions A, 48: 4883-4894. https://doi.org/10.1007/s11661-017-4260-1

[11] Pulsford, C., Jepson, M.A.E., Thomson, R.C., et al. (2022). Microstructural characterisation of creep tested advanced austenitic stainless steel super 304H. Materials at High Temperatures, 39(6): 416-426. https://doi.org/10.1080/09603409.2022.2037328

[12] Kumar, R., Varma, A., Kumar, Y.R., Neelakantan, S., Jain, J. (2022). Enhancement of mechanical properties through modified post-weld heat treatment processes of T91 and Super304H dissimilar welded joint. Journal of Manufacturing Processes, 78: 59-70. https://doi.org/10.1016/j.jmapro.2022.04.008

[13] Hwang, J.H., Song, G.D., Kim, D.W., et al. (2021). Tensile and fatigue properties of Super304H welded joint at elevated temperatures. International Journal of

Fatigue, 143: 105989. https://doi.org/10.1016/j.ijfatigue.2020.105989
[14] Ou, P., Xing, H., Wang, X. et al. (2015). Coarsening and hardening behaviors of Cu-Rich precipitates in Super304H austenitic steel. Metallurgical and Materials Transactions A, 46: 3909-3916. https://doi.org/10.1007/s11661-015-3004-3
[15] Jiang, J., Zhu, L.H. (2012). Strengthening mechanisms of precipitates in S30432 heat-resistant steel during short-term aging. Materials Science and Engineering: A, 539: 170-176. https://doi.org/10.1016/j.msea.2012.01.076
[16] ASTM International. (2018). Standard test methods for notched bar impact testing of metallic materials (ASTM E23-18). https://doi.org/10.1520/E0023-18
[17] ASTM International. (2022). Standard test method for microindentation hardness of materials (ASTM E384-22). https://doi.org/10.1520/E0384-22
[18] Alkhafaji, M.M., Mohammed, M.S., Amin, S.A., Habeeb, L.J., Majdi, H.S. (2025). Electrodes' effects on welding of copper to 304 stainless steel and analysis of heat distribution, microstructures, and mechanical properties. International Journal of Computational Methods and Experimental Measurements, 13(1): 85-96. https://doi.org/10.18280/ijcmem.130109
[19] Zieliński, A., Wersta, R., Sroka, M. (2021). Analysis of the precipitation process of secondary phases after long-term ageing of S304H steel. Bulletin of the Polish Academy of Sciences Technical Sciences, 69(5): e137520. https://doi.org/10.24425/bpasts.2021.137520
[20] Hamdey, M.D., Mohammed, M.S., Kareem, A.H., Majdi, H.S. (2024). Thermal and mechanical analysis in joint welding of thick steel alloy plates with and without backing plate. Journal of Engineering Science and Technology, 19(5): 1974-1989.
[21] Hatakeyama, T., Sawada, K., Sekido, K., Hara, T., Kimura, K. (2022). Microstructural factors of the complex creep rate change in 18Cr-9Ni-3Cu-Nb-N steel. Materials Science and Engineering: A, 831: 142225. https://doi.org/10.1016/j.msea.2021.142225
[22] Idan, A.F.I., Falih, D.A., Mohammed, M.S., Kareem, A.H., Majdi, H.S. (2025). Experimental investigation of welding technology effects on ASTM A516 Grade 70 welding joint microstructure, corrosion resistance, and mechanical properties. Journal Européen des Systèmes Automatisés, 58(10): 2055-2070. https://doi.org/10.18280/jesa.581006
[23] San, X.Y., Zhang, B., Wu, B., Wei, X.X., Oguzie, E.E., Ma, X.L. (2018). Investigating the effect of Cu-rich phase on the corrosion behavior of Super 304H austenitic stainless steel by TEM. Corrosion Science, 130: 143-152. https://doi.org/10.1016/j.corsci.2017.11.001
[24] Liu, Z., Wang, X.T., Dong, C. (2020). Effect of boron on G115 Martensitic heat resistant steel during aging at 650 °C. (2020). Materials Science and Engineering: A, 787: 139529. https://doi.org/10.1016/j.msea.2020.139529
[25] Hatakeyama, T., Sawada, K. (2024). Precipitation behavior of the M23C6 phase on the coherent twin boundary of 25Cr-20Ni-Nb-N steel. Materials Letters, 363: 136277. https://doi.org/10.1016/j.matlet.2024.136277
[26] Zhou, Q.W., Wang, R.K., Zheng, Z.J., Gao, Y. (2018). Interpretation for the fast sigma phase precipitation in the high intensity shot peened nanocrystalline Super304H stainless steel. Applied Surface Science, 462: 804-814. https://doi.org/10.1016/j.apsusc.2018.08.097
[27] Horváth, J., Janovec, J., Junek, M. (2016). The changes in mechanical properties of austenitic creep resistant steels Super 304H and HR3C caused by medium-term isothermal ageing. Solid State Phenomena, 258: 639-642. https://doi.org/10.4028/www.scientific.net/SSP.258.639
[28] Parnian, N. (2012). Failure analysis of austenitic stainless steel tubes in a gas fired steam heater. Materials & Design (1980-2015), 36: 788-795. https://doi.org/10.1016/j.matdes.2011.12.027
[29] Ramkumar, K.D., Arivazhagan, N., Narayanan, S. (2012). Effect of filler materials on the performance of Gas Tungsten arc-welded AISI 304 and Monel 400. Materials & Design, 40: 70-79. https://doi.org/10.1016/j.matdes.2012.03.024
[30] Djeloud, H., Moussaoui, M., Kouider, R., Al-Kassir, A., Carrasco-Amador, J.P. (2023). Study of the heat exchange and relaxation conditions of residual stresses due to welding of austenitic stainless steel. Energies, 16(7): 3176. https://doi.org/10.3390/en16073176
[31] Zhou, Y.H., Liu, C.X., Liu, Y.C., Guo, Q.Y., Li, H.J. (2016). Coarsening behavior of MX carbonitrides in type 347H heat-resistant austenitic steel during thermal aging. International Journal of Minerals, Metallurgy, and Materials, 23: 283-293. https://doi.org/10.1007/s12613-016-1237-9
[32] Lolla, T., Siefert, J., West, G., Gagliano, M. (2019). A study of sigma phase evolution in long-term creep-tested Super 304H samples. In Joint EPRI – 123HiMAT International Conference on Advances in High Temperature Materials, Nagasaki, Japan, pp. 726-737. https://doi.org/10.31399/asm.cp.am-epri-2019p0726
[33] Xie, F., Zhu, W.H., Zheng, Z.J., Gao, Y. (2017). Influence of high temperature softening and solid solution on intergranular corrosion susceptibility of Super304H stainless steel. Corrosion Engineering, Science and Technology: The International Journal of Corrosion Processes and Corrosion Control, 52(4): 302-310. https://doi.org/10.1080/1478422X.2016.1277322
[34] Ji, Y.S., Park, J., Lee, S.Y., et al. (2017). Long-term evolution of σ phase in 304H austenitic stainless steel: Experimental and computational investigation. Materials Characterization. 128: 23-29. https://doi.org/10.1016/j.matchar.2017.03.030
[35] Liu, J.B., Chen, C.X., Feng, Q., et al. (2017). Dislocation activities at the martensite phase transformation interface in metastable austenitic stainless steel: An in-situ TEM study. Materials Science and Engineering: A, 703: 236-243. https://doi.org/10.1016/j.msea.2017.06.107
[36] He, J., Wang, Q., Zhang, H., et al. (2018). Dynamic deformation behavior of a face-centered cubic FeCoNiCrMn high-entropy alloy. Science Bulletin, 63(6): 362-368. https://doi.org/10.1016/j.scib.2018.01.022